Supporting Information

For

π-Bond Character in Metal-Alkyl Compounds for C–H Activation: How, When and Why?

Christopher P. Gordon,[1] Damien B. Culver,[2] Matthew P. Conley,[2] Odile Eisenstein,[3,4] Richard A. Andersen,[5] Christophe Copéret[1,*]

[1] Department of Chemistry and Applied Biosciences, ETH Zürich, Vladimir Prelog Weg 1-5, 8093, Zürich, Switzerland.

[2] Department of Chemistry, University of California, Riverside, California 92521, United States.

[3] Institut Charles Gerhardt, UMR 5253 CNRS-UM-ENSCM, Université de Montpellier, 34095 Montpellier, France.

[4] Hylleraas Centre for Quantum Molecular Sciences, Department of Chemistry, University of Oslo, P.O. Box 1033, Blindern, 0315 Oslo, Norway.

[5] Department of Chemistry, University of California, Berkeley, California 94720, United States.

Contents

1. Experimental section

NMR Measurements

The solid-state ^{1}H and ^{13}C NMR spectra were obtained on Bruker Avance III 600 MHz spectrometer, using a 3.2 mm probe, and the magnetic fields were externally referenced by setting the downfield ^{13}C signal of adamantane to 38.4 ppm. The samples were loaded in a 3.2 mm sapphire rotor closed with a zirconia cap with a Teflon insert placed between the sample and the cap to prevent sample spill.

Cross polarization magic angle spinning (CPMAS) and spin echo type experiments were used to measure ^{13}C and ^{1}H spectra, respectively. The ^{1}H excitation and decoupling radiofrequency (rf) fields were set to 100 kHz. For CPMAS measurements, the CP condition was optimized to match the Hartmann-Hahn condition under MAS with minor adjustments to reach the best CP efficiency experimentally.

Synthesis of organometallic compounds

$Cp^*_2Sc–CH_3$ was synthesized according to literature procedure.[1]

2. Computational Details

All geometry optimizations were performed without any symmetry constraints using the Gaussian09 package[2] with the PBE0 functional[3]. Sc, Y, Lu, Ti, Zr, W, and Ir were represented by the quasi-relativistic effective core potential (RECP) from the Stuttgart group and the associated basis sets.[4]-[6] The remaining atoms (H, C, O, F, P, S) were represented by a triple-ζ pcseg-2 basis set.[7] The nature of stationary points (minima or transition states) was verified by analytical Hessian calculations. Statistical mechanics calculations were carried out using the rigid rotor/harmonic oscillator approximations (298 K, 1 atm).

NMR calculations were performed within the GIAO framework using ADF 2014[8] with the PBE0 functional and Slater-type basis sets of triple-ζ quality (TZ2P). Relativistic effects were treated by the 2 component zeroth order regular approximation (ZORA).[9]-[13] Analysis of scalar-relativistic natural localized molecular orbitals were done with the NBO 6.0 program.[14] Calculated NMR shielding tensors were analyzed using these scalar-relativistic NLMO.[15]-[18] The 3D representation of the calculated shielding tensors were obtained as polar plots[19],[20] of functions $\sum_{ij} r_i \sigma_{ij} r_j$, with a scaling factor of 0.5.

Electronic energies were refined as single point calculations from the optimized structures, using GD3 dispersion corrections[21] and the SMD model[22] to account for the solvent (toluene).

The Gibbs energy (G) and enthalpy (H) was estimated as:

$$G^{toluene,PBE0,D3} = E^{toluene,PBE0,D3} + G^{gas,PBE0} - E^{gas,PBE0}$$

$$H^{toluene,PBE0,D3} = E^{toluene,PBE0,D3} + H^{gas,PBE0} - E^{gas,PBE0}$$

3. Solid-State NMR Spectra

$Cp^*_2Sc–CH_3$

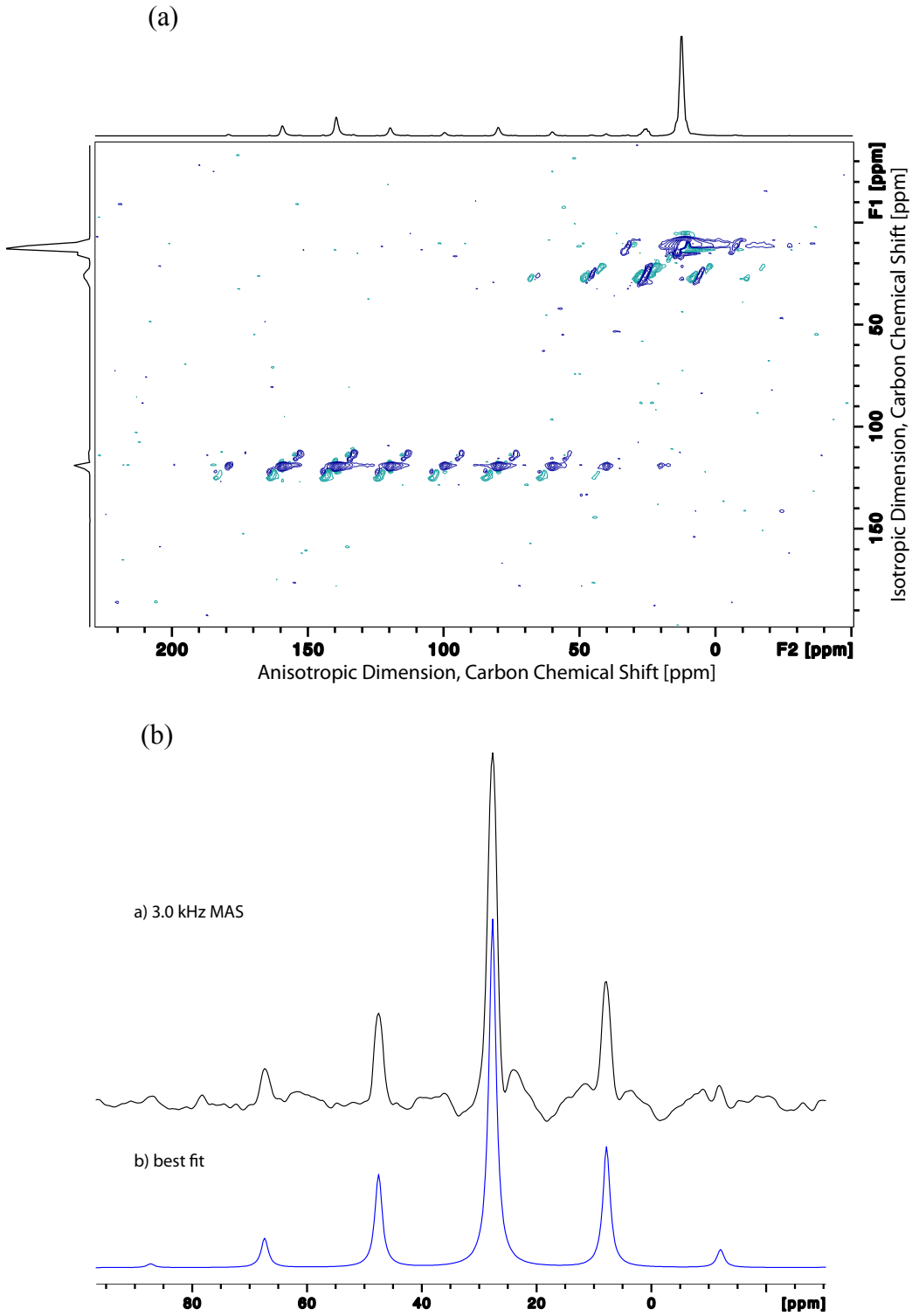

Figure S1. (a) The CP magic-angle turning[23] (CP-MAT, 14.1 T at 100 K) spectrum of **$Cp^*_2Sc–CH_3$** at a spinning rate of 3.0 kHz. The contact time for CP was 0.5 ms, and the recycle delay was 1 s. 72 scans per *t1* increment and 713 *t1* increments were acquired. (b) Blue: the spectrum of the spinning side bands for the α-carbon, which were obtained by slicing horizontally the CP-MAT spectrum at 28 ppm. Black: best-fit simulated spinning side bands of the corresponding carbon (δ_{iso} = 28 ppm, δ_{11} = 64 ppm, δ_{22} = 22 ppm, δ_{33} = -3 ppm).

4. NMR Calculations

Table S1: Calculated shielding tensors (all values in ppm).

	σ_{iso}	σ_{11}	σ_{22}	σ_{33}	δ_{iso}	δ_{11}	δ_{22}	δ_{33}
$Cp^*_2Sc–CH_3$	163	124	178	187	28	67	13	4
$Cp^*_2Lu–CH_3$	170	138	181	190	21	53	10	1
$Cp^*_2Y–CH_3$	169	134	183	190	22	57	8	1
$[Cp^*_2Ti–CH_3]^+$	94	-27	133	178	97	218	58	13
$[Cp_2Zr–CH_3]^+$	90	-65	128	206	101	256	63	-15
$Cp^*(CO)_2W–CH_3$	48	-136	65	214	143	326	126	-23
$Cp^*(CO)Fe–CH_3$	104	-121	148	286	87	312	43	-95
$[Cp^*(PMe_3)Ir–CH_3]^+$	157	68	156	247	34	123	35	-56

Table S2: Diamagnetic and paramagnetic contributions to shielding (all values in ppm).

	σ_{11}		σ_{22}		σ_{33}	
	σ_{dia}	σ_{para}	σ_{dia}	σ_{para}	σ_{dia}	σ_{para}
$Cp^*_2Sc–CH_3$	216	-92	227	-50	213	-26
$Cp^*_2Lu–CH_3$	215	-76	213	-31	229	-39
$Cp^*_2Y–CH_3$	225	-90	221	-38	231	-42
$[Cp^*_2Ti–CH_3]^+$	217	-244	231	-98	213	-35
$[Cp_2Zr–CH_3]^+$	223	-288	232	-104	221	-15
$Cp^*(CO)_2W–CH_3$	222	-358	230	-165	213	0
$Cp^*(CO)Fe–CH_3$	222	-343	223	-76	213	73
$[Cp^*(PMe_3)Ir–CH_3]^+$	216	-148	221	-65	216	32

Table S3: NCS analysis of metal alkyl compounds – σ_{11} (most deshielded component; all values in ppm).

	σ_{11}	σ_{dia}	σ_{para}	components of σ_{para}			
				σ(M-C)	σ(C-H)	σ(C-H')	σ(C-H'')
$Cp^*_2Sc–CH_3$	124	216	-92	-113	8	5	8
$Cp^*_2Lu–CH_3$	138	215	-76	-109	20	14	17
$Cp^*_2Y–CH_3$	134	225	-90	-93	2	7	0
$[Cp^*_2Ti–CH_3]^+$	-27	217	-244	-180	-40	-9	-14
$[Cp_2Zr–CH_3]^+$	-65	223	-288	-182	-29	-29	-30
$Cp^*(CO)_2W–CH_3$	-136	222	-358[a]	-220	-21	-32	-24
$Cp^*(CO)Fe–CH_3$	-121	222	-343[b]	-223	22	30	-52
$[Cp^*(PMe_3)Ir–CH_3]^+$	68	216	-148	-102	-1	-6	5

[a] a contribution of -26 ppm arises from a carbon core orbital CR(C). [b] a contribution of -88 ppm arises from a carbon core orbital CR(C).

Table S4: NCS analysis of metal alkyl compounds – σ_{22} (all values in ppm).

	σ_{22}	σ_{dia}	σ_{para}	components of σ_{para}			
				σ(M-C)	σ(C-H)	σ(C-H')	σ(C-H'')
$Cp^*_2Sc–CH_3$	178	227	-50	-3	-16	-16	-6
$Cp^*_2Lu–CH_3$	181	213	-31	-63	8	13	25
$Cp^*_2Y–CH_3$	183	221	-38	-48	8	-4	9
$[Cp^*_2Ti–CH_3]^+$	133	231	-98	-2	-10	-32	-27
$[Cp_2Zr–CH_3]^+$	128	232	-104	-8	-44	-44	3
$Cp^*(CO)_2W–CH_3$	65	230	-165	-12	-78	13	-88
$Cp^*(CO)Fe–CH_3$	148	223	-76	2	-67	12	-13
$[Cp^*(PMe_3)Ir–CH_3]^+$	156	221	-65	-4	-17	0	-28

Table S5: NCS analysis of metal alkyl compounds – σ_{33} (most shielded component; all values in ppm).

	σ_{33}	σ_{dia}	σ_{para}	components of σ_{para}			
				σ(M-C)	σ(C-H)	σ(C-H')	σ(C-H'')
$Cp^*_2Sc–CH_3$	187	213	-26	-58	15	11	10
$Cp^*_2Lu–CH_3$	190	229	-39	-7	1	-13	-13
$Cp^*_2Y–CH_3$	190	231	-42	0	-11	-14	-12
$[Cp^*_2Ti–CH_3]^+$	178	213	-35	-48	2	4	7
$[Cp_2Zr–CH_3]^+$	206	221	-15	-32	13	9	-10
$Cp^*(CO)_2W–CH_3$	214	213	0	-28	14	-16	13
$Cp^*(CO)Fe–CH_3$	286	213	73	33	-5	-14	25
$[Cp^*(PMe_3)Ir–CH_3]^+$	247	216	32	-17	2	2	8

5. Graphical Representation of the Results of the Natural Chemical Shift Analysis

The histograms below show the decomposition of the principal components of the shielding tensor (σ_{11}, σ_{22}, and σ_{33}) into diamagnetic and paramagnetic contributions. The paramagnetic contributions are further decomposed into the contributions of individual NLMOs.

Figure S2. Orbital analysis of the σ_{11} component of the α-carbons of $Cp^*_2Sc\text{-}CH_3$, $Cp^*_2Lu\text{-}CH_3$, $Cp^*_2Y\text{-}CH_3$, $[Cp^*_2Ti\text{-}CH_3]^+$, $Cp^*(CO)_2W\text{-}CH_3$, $Cp(CO)Fe\text{-}CH_3$, and $Cp^*(Me_3P)_2Ir\text{-}CH_3$.

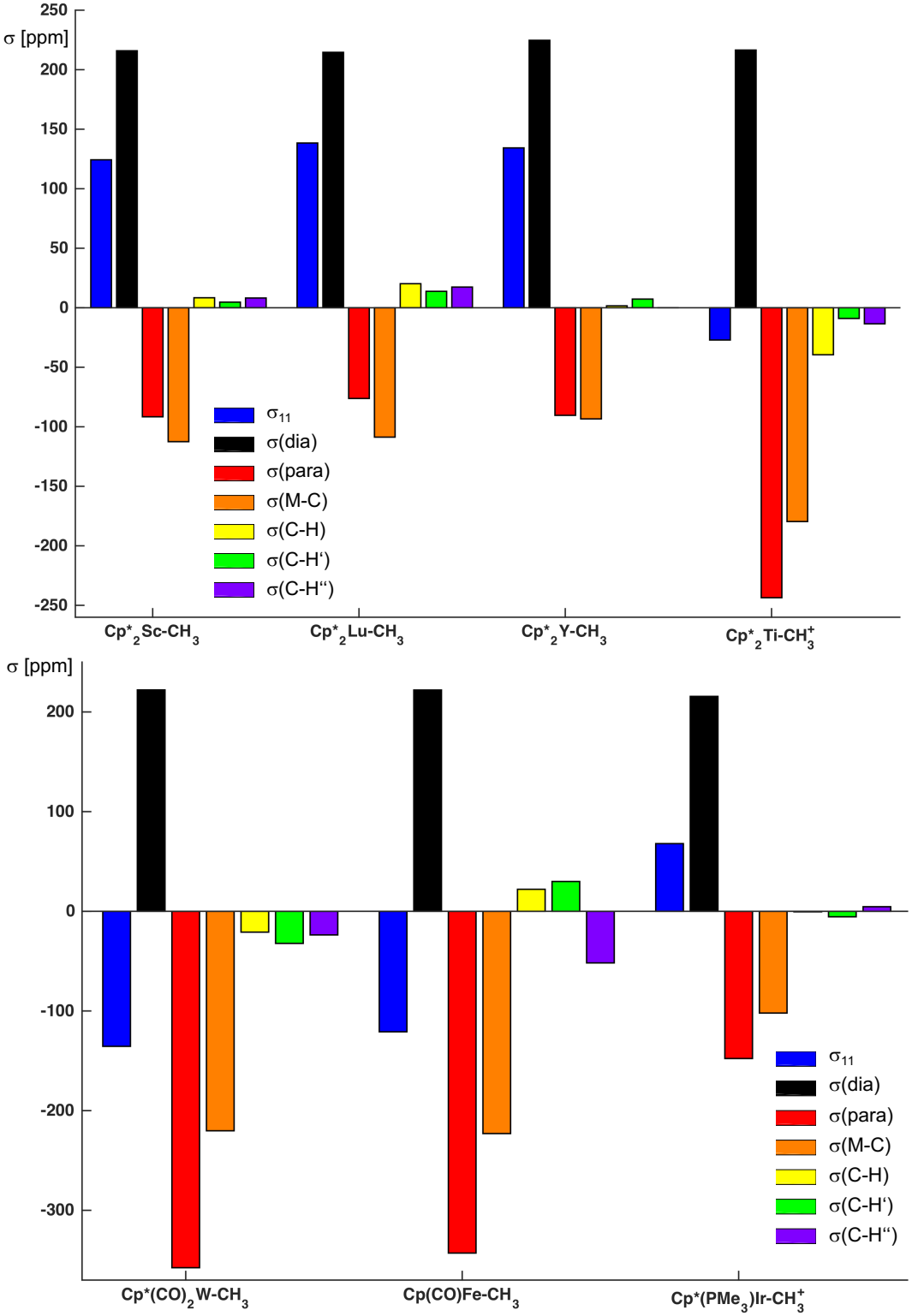

Figure S3. Orbital analysis of the σ_{22} component of the α-carbons of $Cp^*_2Sc\text{-}CH_3$, $Cp^*_2Lu\text{-}CH_3$, $Cp^*_2Y\text{-}CH_3$, $[Cp^*_2Ti\text{-}CH_3]^+$, $Cp^*(CO)_2W\text{-}CH_3$, $Cp(CO)Fe\text{-}CH_3$, and $Cp^*(Me_3P)_2Ir\text{-}CH_3$.

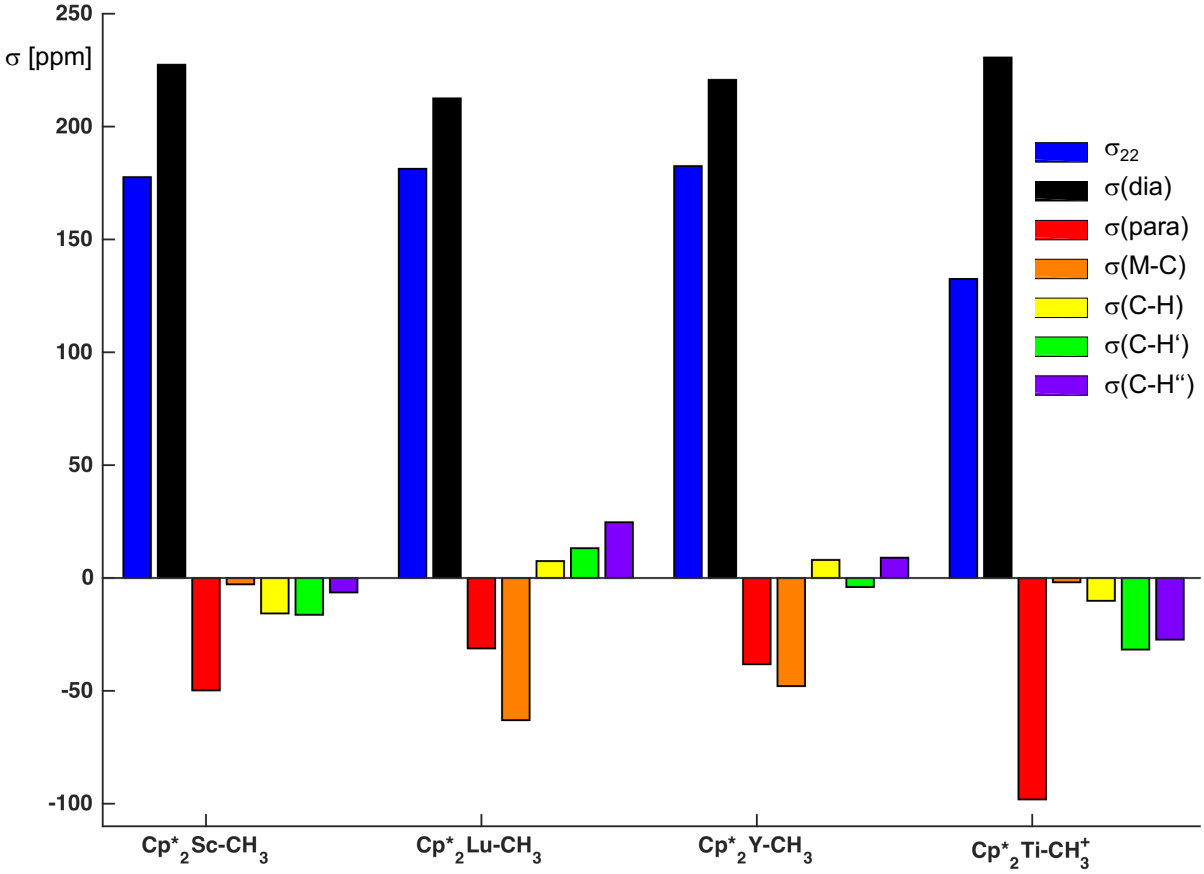

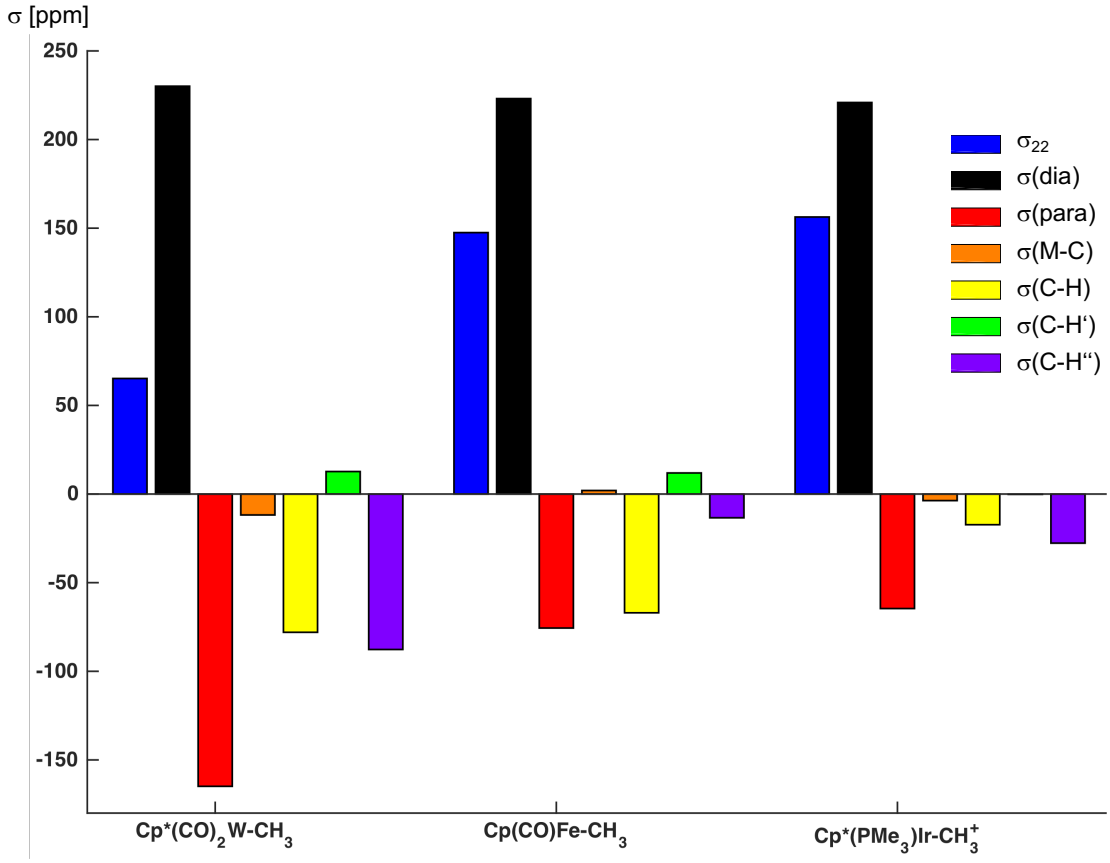

Figure S4. Orbital analysis of the σ_{33} component of the α-carbons of $Cp^*_2Sc\text{-}CH_3$, $Cp^*_2Lu\text{-}CH_3$, $Cp^*_2Y\text{-}CH_3$, $[Cp^*_2Ti\text{-}CH_3]^+$, $Cp^*(CO)_2W\text{-}CH_3$, $Cp(CO)Fe\text{-}CH_3$, and $Cp^*(Me_3P)_2Ir\text{-}CH_3$.

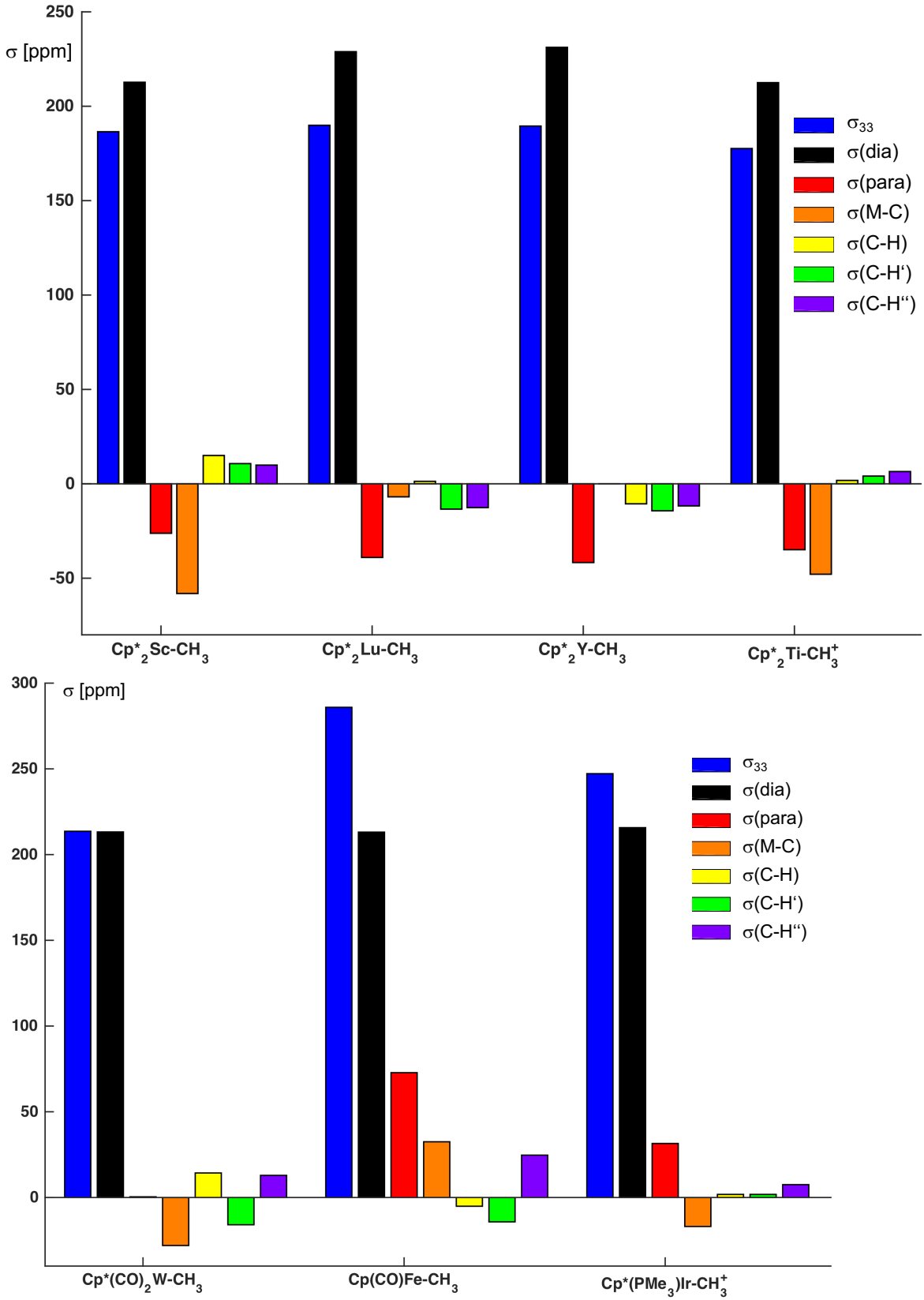

6. Structural and NMR-Spectroscopic Properties of Catalyst Precursors

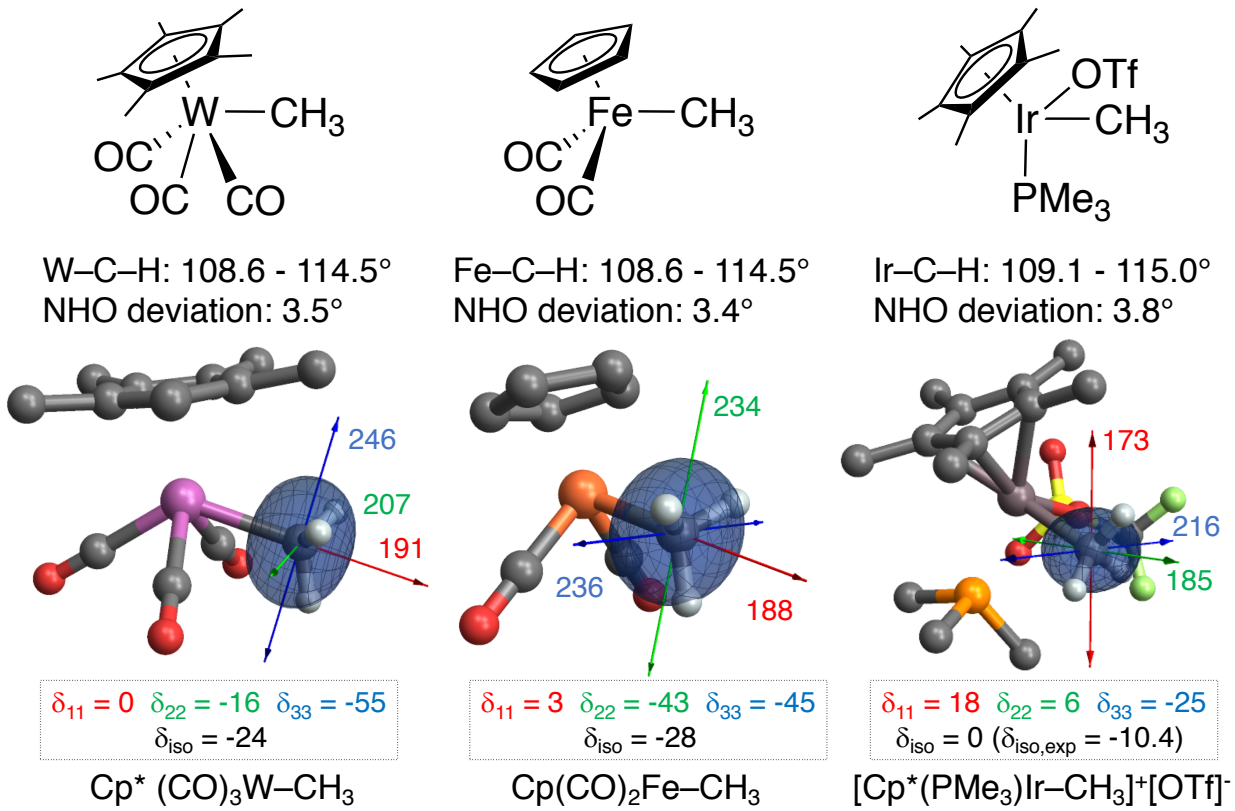

Figure S5. M–C–H angles, deviation of the natural hybrid orbital directionality from the M–C axis, orientation of shielding tensors, and chemical shift values of the catalyst precursors $Cp^*(CO)_3W–CH_3$, $Cp(CO)_2Fe–CH_3$, and $[Cp^*(PMe_3)Ir–CH_3]^+[OTf]^-$. Chemical shift and shielding values are given in ppm. The M–C–H angles for the W- and Fe-based compounds are indeed calculated to be similar.

7. Shielding Tensors of Cp_2TiMe_2, $Cp_2TiMeCl$, Cp_2MoMe_2 and $[Cp_2ZrMe]^+$

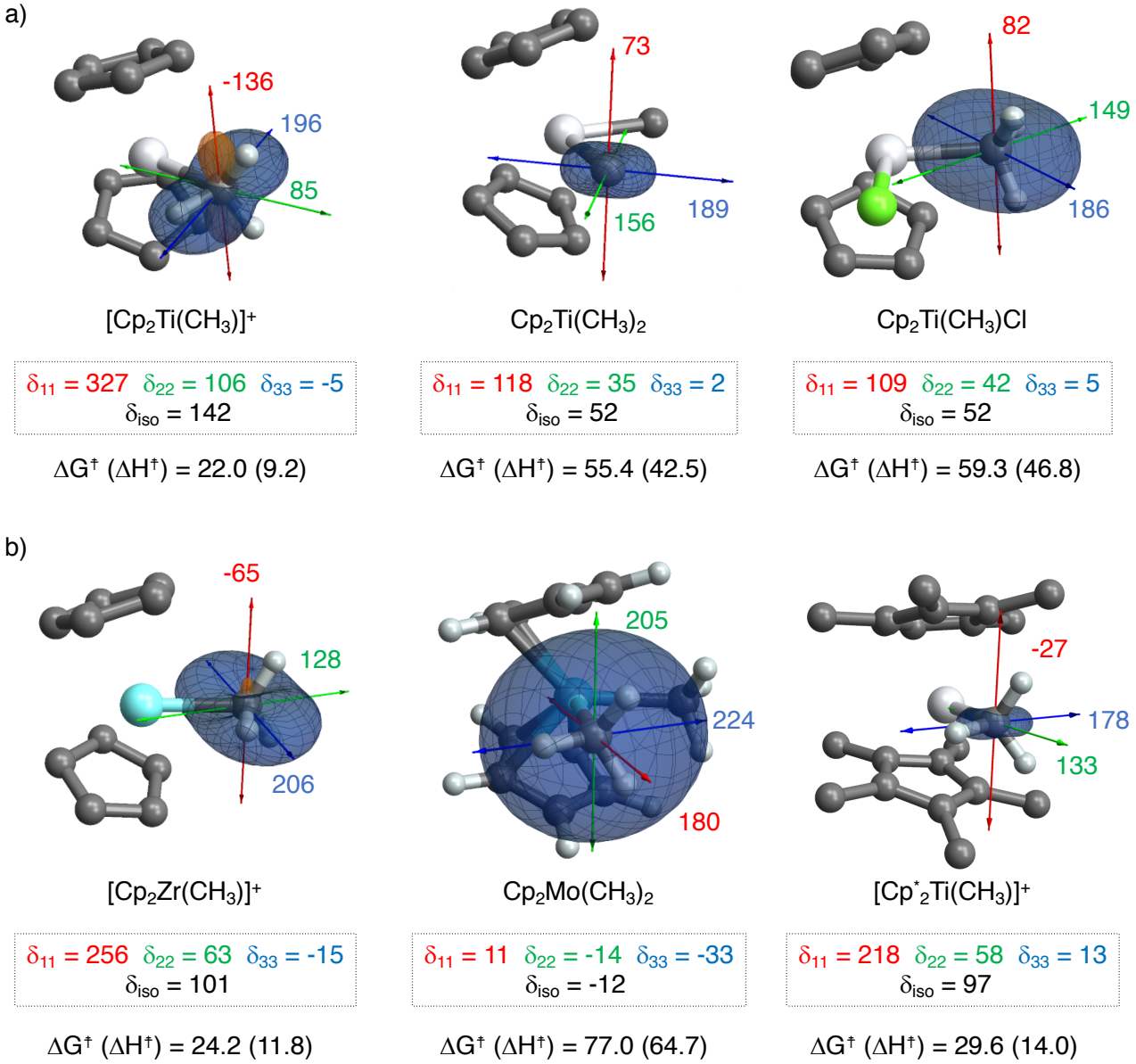

Figure S6. Shielding tensors, associated chemical shifts and free energy (enthalpy) barriers for methyl-methane exchange in a) $[Cp_2Ti(CH_3)]^+$, $Cp_2Ti(CH_3)_2$, $Cp_2Ti(CH_3)Cl$ and b) $[Cp_2Zr(CH_3)]^+$, $Cp_2Mo(CH_3)_2$, and $[Cp^*_2Ti(CH_3)]^+$. All chemical shielding/shift values are given in ppm. Transition state energy values are given in kcal mol^{-1} with respect to separated reactants (metal complex + CH_4).

8. Optimized Structures of all Calculated Species

Optimized Structures of all species are provided as .xyz files as supplementary material.

9. References

[1] Thompson, M. E.; Baxter, S. M.; Bulls, A. R.; Burger, B. J.; Nolan, M. C.; Santarsiero, B. D.; Schaefer, W. P.; Bercaw, J. E., σ-Bond Metathesis for Carbon-Hydrogen Bonds of Hydrocarbons and Sc-R (R = H, Alkyl, Aryl) Bonds of Permethylscandocene Derivatives. Evidence for Noninvolvement of the π System in Electrophilic Activation of Aromatic and Vinylic C-H bonds *J. Am. Chem. Soc.* **1987**, *109*, 203-219.

[2] Frisch, M. J.; Trucks, G. W.; Schlegel, H. B.; Scuseria, G. E.; Robb, M. A.; Cheeseman, J. R.; Scalmani, G.; Barone, V.; Mennucci, B.; Petersson, G. A.; Nakatsuji, H.; Caricato, M.; Li, X.; Hratchian, H. P.; Izmaylov, A. F.; Bloino, J.; Zheng, G.; Sonnenberg, J. L.; Hada, M.; Ehara, M.; Toyota, K.; Fukuda, R.; Hasegawa, J.; Ishida, M.; Nakajima, T.; Honda, Y.; Kitao, O.; Nakai, H; Vreven, T.; Montgomery, J. A.; Peralta, Jr. J. E.; Ogliaro, F.; Bearpark, M.; Heyd, J. J.; Brothers, E.; Kudin, K. N.; Staroverov, V. N.; Kobayashi, R.; Normand, J.; Raghavachari, K.; Rendell, A.; Burant, J. C.; Iyengar, S. S.; Tomasi, J.; Cossi, M.; Rega, N.; Millam, J. M.; Klene, M.; Knox, J. E.; Cross, J. B.; Bakken, V.; Adamo, C.; Jaramillo, J.; Gomperts, R.; Stratmann, R. E.; Yazyev, O.; Austin, A. J.; Cammi, R.; Pomelli, C.; Ochterski, J. W.; Martin, R. L.; Morokuma, K.; Zakrzewski, V. G.; Voth, G. A.; Salvador, P.; Dannenberg, J. J.; Dapprich, S.; Daniels, A. D.; Farkas, Ö.; Foresman, J. B.; Ortiz, J. V.; Cioslowski, J.; Fox, D. J. *Gaussian 09* (Gaussian, Inc., Wallingford CT, 2009) VERSION D.01.

[3] Adamo, C.; Barone, V., Toward Reliable Density Functional Methods Without Adjustable Parameters: The PBE0 Model. *J. Chem. Phys.* **1999**, *110*, 6158-6170.

[4] Dolg, M.; Wedig, U.; Stoll, H.; Preuss, H., Energy-Adjusted ab Initio Pseudopotentials for the First Row Transition Elements. *J. Chem. Phys.* **1987**, *86*, 866-872.

[5] Andrae, D.; Haeussermann, U.; Dolg, M.; Stoll, H.; Preuss, H., Energy-Adjusted ab Initio Pseudopotentials for the Second and Third Row Transition Elements. *Theor. Chim. Acta* **1990**, *77*, 123-141.

[6] Martin, J. M. L.; Sundermann, A., Correlation Consistent Valence Basis Sets for Use with the Stuttgart–Dresden–Bonn Relativistic Effective Core Potentials: The Atoms Ga–Kr and In–Xe. *J. Chem. Phys.* **2001**, *114*, 3408-3420.

[7] Jensen, J., Unifying General and Segmented Contracted Basis Sets. Segmented Polarization Consistent Basis Sets. *J. Chem. Theory Comput.*, **2014**, *10*, 1074-1085.

[8] te Velde, G.; Bickelhaupt, F. M.; Baerends, E. J.; Fonseca Guerra, C.; van Gisbergen, S. J. A.; Snijders, J. G.; Ziegler T. *J. Comp. Chem.* **2001**, *22*, 931. Amsterdam Density Functional (ADF) Theoretical Chemistry Vrieje Universitet see http://www.scm.com (VERSION 2014).

[9] van Lenthe, E.; Baerends, E. J.; Snijders, J. G., Relativistic Regular Two-Component Hamiltonians. *J. Chem. Phys.* **1993**, *99*, 4597-4610.

[10] van Lenthe, E.; Baerends E. J.; Snijders, J. G., Relativistic Total Energy Using Regular Approximations. *J. Chem. Phys.* **1994**, *101*, 9783-9792.

[11] van Lenthe, E.; Baerends E. J.; Snijders, J. G., Geometry Optimizations in the Zero Order Regular Approximation for Relativistic Effects. *J. Chem. Phys.* **1999**, *110*, 8943-8953.

[12] van Lenthe, E.; Baerends, E. J.; Snijders, J. G., The Zero-Order Regular Approximation for Relativistic Effects: The Effect of Spin-Orbit Coupling in Closed Shell Molecules. *J. Chem. Phys.* **1996**, *105*, 6505-6516.

[13] van Lenthe, E.; van Leeuwen, R.; Baerends, E. J.; Snijders, J. G., Relativistic Regular Two-Component Hamiltonians. *Int. J. Quant. Chem.* **1996**, *57*, 281-293.

[14] Glendening, E. D.; Badenhoop, J. K.; Reed, A. E.; Carpenter, J. E.; Bohmann, J. A.; Morales, C. M.; Landis, C. R.; Weinhold, F.; Theoretical Chemistry Institute, University of Wisconsin, Madison, WI, USA **2013**, http://nbo6.chem.wisc.edu/

[15] Bohmann, J. A.; Weinhold, F.; Farrar, T. C. J., Natural Chemical Shielding Analysis of Nuclear Magnetic Resonance Shielding Tensors from Gauge-Including Atomic Orbital Calculations. *J. Chem. Phys.* **1997**, *107*, 1173-1184.

[16] Autschbach, J.; Zheng, T., Analyzing Pt Chemical Shifts Calculated from Relativistic Density Functional Theory Using Localized Orbitals: The Role of Pt 5d Lone Pairs. *Magn. Reson. Chem.* **2008**, *46*, S45-55.
[17] Autschbach, J., Analyzing NMR Shielding Tensors Calculated With Two-Component Relativistic Methods Using Spin-Free Localized Molecular Orbitals. *J. Chem. Phys.* **2008**, *128*, 164112.
[18] Aquino, F.; Pritchard, B.; Autschbach, J., Scalar Relativistic Computations and Localized Orbital Analyses of Nuclear Hyperfine Coupling and Paramagnetic NMR Chemical Shifts. *J. Chem. Theory Comput.* **2012**, *8*, 598-609.
[19] Autschbach, J.; Zheng, S.; Schurko, R.W., Analysis of Electric Field Gradient Tensors at Quadrupolar Nuclei in Common Structural Motifs. *Concepts Magn Reson Part A.* **2010**, *36A*, 84-126.
[20] Zurek, E.; Pickard, C. J.; Autschbach, J., Density Functional Study of the ^{13}C NMR Chemical Shifts in Single-Walled Carbon Nanotubes with Stone-Wales Defects. *J. Phys. Chem. C.* **2008**, *112*, 11744-11750.
[21] Grimme, S.; Antony, J.; Ehrlich, S.; Krieg, H., A Consistent and Accurate ab Initio Parametrization of Density Functional Dispersion Correction (DFT-D) for the 94 Elements H-Pu *J. Chem. Phys.* **2010,** *132*, 154104.
[22] Marenich, A. V.; Cramer, C. J.; Truhlar, D. G., Universal Solvation Model Based on Solute Electron Density and on a Continuum Model of the Solvent Defined by the Bulk Dielectric Constant and Atomic Surface Tensions. *J. Phys. Chem. B* **2009,** *113*, 6378-6396.
[23] Bax, A.; Szeverenyi, N. M.; Maciel, G. E., Correlation of Isotropic Shifts and Chemical Shift Anisotropies by Two-Dimensional Fourier-Transform Magic-Angle Hopping NMR Spectroscopy. *J. Magn. Reson.* **1983**, *52*, 147-152.